Supporting Information

``

Synthesis of $CsPbBr_3$ Decorated ZIF-8 Nanocomposite for Enhanced Photocatalytic Performance

Alen Sam Thomas[1], Philip Nathaniel Immanuel[1] Neena Prasad[1], Achiad Goldreich[1], Jonathan Prilusky[1], Raanan Carmieli[2], Lena Yadgarov [1],*

[1] Department of Chemical Engineering, Ariel University, Israel. 4070000

[2]Department of Molecular Chemistry and Materials Science, Weizmann Institute of Science, Rehovot, Israel, 7610001.

**Corresponding Author: lenay@ariel.ac.il*

1) Particle size distribution

The size distribution of nanocrystals was analyzed using ImageJ software from TEM and SEM images. For $CsPbBr_3$ nanocrystals (CPB NCs), particle size was determined using Fast Fourier Transform (FFT) analysis, which converts spatial patterns into frequency domain data for precise measurement of periodic structures. For the remaining particles, size measurements were obtained through line profiling, where the scale was first set for the image, followed by manually drawing lines on individual particles to determine their size. The extracted data were then plotted using Origin software to generate a size distribution graph.

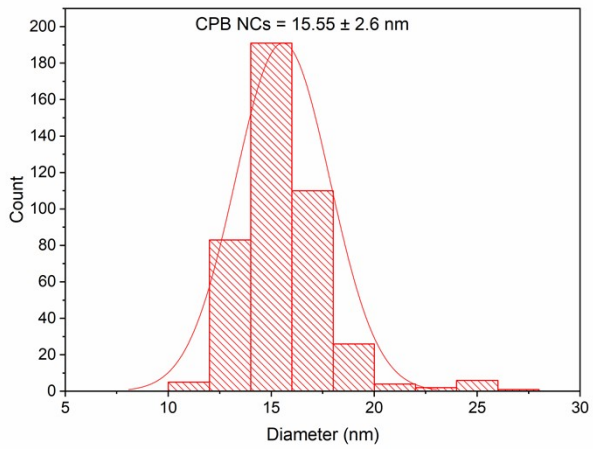

Figure S1: The calculated particle size distribution of $CsPbBr_3$-NCs (CPB-NCs) using the ImageJ analytical tool.

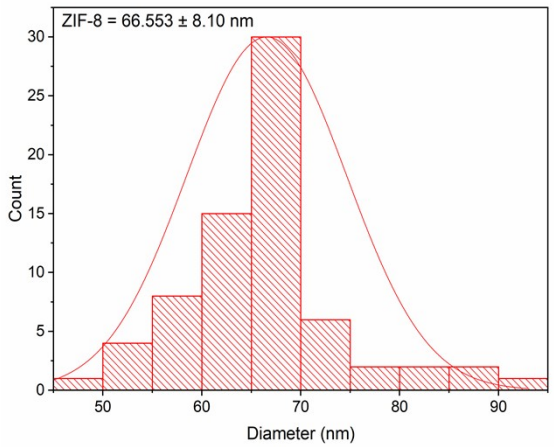

Figure S2: The calculated particle size distribution of Zeolidic imidazole framework-8 (ZIF-8). The calculation was done using the ImageJ analytical tool.

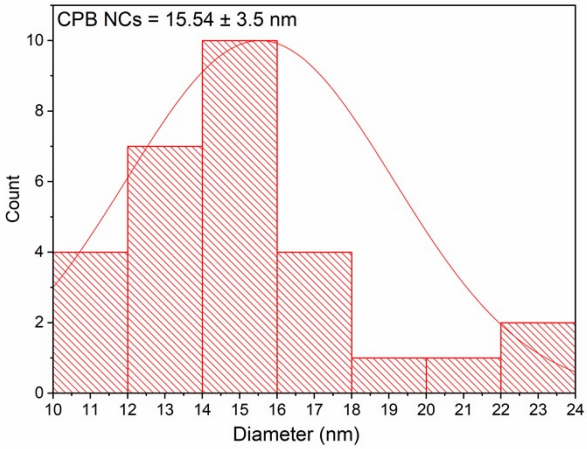

Figure S3: The calculated particle size distribution of CPB NCs on ZIF-8 using the ImageJ analytical tool.

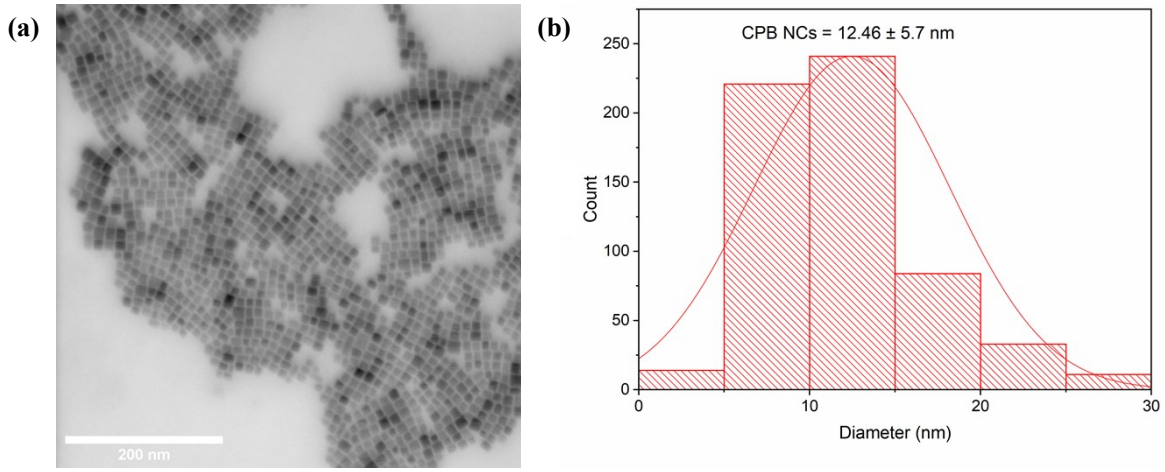

Figure S4: (a) STEM micrograph of CPB NCs in the supernatant after the reaction (b) the calculated particle size distribution of CPB NCs using the ImageJ analytical tool. *The samples were prepared using the supernatant obtained from the centrifuged solution of CPB NCs.*

The transmission electron microscope (TEM) images of the CPB/ZIF-8 composites are shown in Figure S5. The CPB NCs appear darker in the images due to the higher atomic number and molecular weight of lead (Pb) compared to zinc (Zn). Heavier elements scatter more electrons, resulting in greater contrast in TEM images, making Pb-based particles appear darker. Thus, the darker spots correspond to CPB NCs, while the larger, lighter particles represent ZIF-8. The area of the marked particles was calculated using ImageJ software. The process involved setting the scale of the TEM micrograph and then manually outlining each particle using the Freehand Selection tool to trace its shape precisely. The software then computed the particle areas tabulated in Table S1.

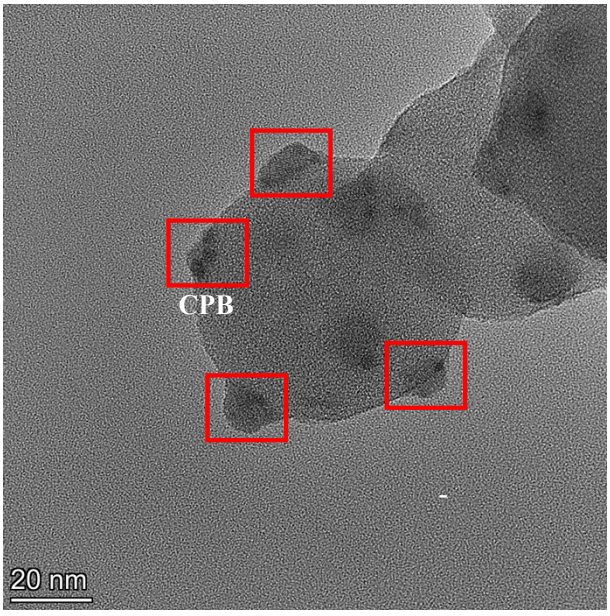

Figure S5*: TEM image of the CPB/ZIF-8 (The CPB NCs on ZIF-8 are marked in red)*

Table S1: Area of the different particles in CPB/ZIF-8 composite by ImageJ software

Particle	Area
ZIF-8	3436.988 nm^2
CPB NCs	625.09 nm^2 (18.18%)

2) Absorption spectra and optical band gap

The optical band gap of the materials was calculated using Tauc's plot, where $(\alpha h\nu)^n$ is plotted against photon energy ($h\nu$). The absorption coefficient (α) was determined from the UV-Vis absorption spectrum using the equation $\alpha = (2.303 \times A) / d$, where A is the absorbance, and d is the path length. The band gap was obtained by extrapolating the linear region of the $(\alpha h\nu)^n$ vs. $h\nu$ plot to the x-axis, with n = 2 for direct band gap semiconductors and n = ½ for indirect band gap materials.

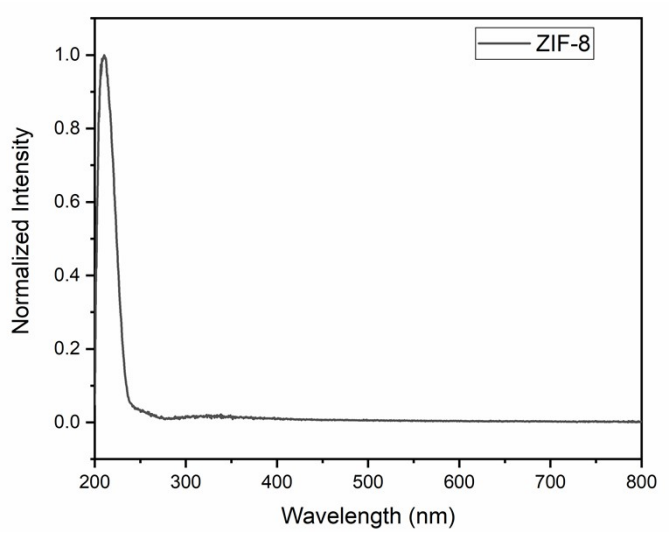

Figure S6: Absorption Spectra of ZIF-8

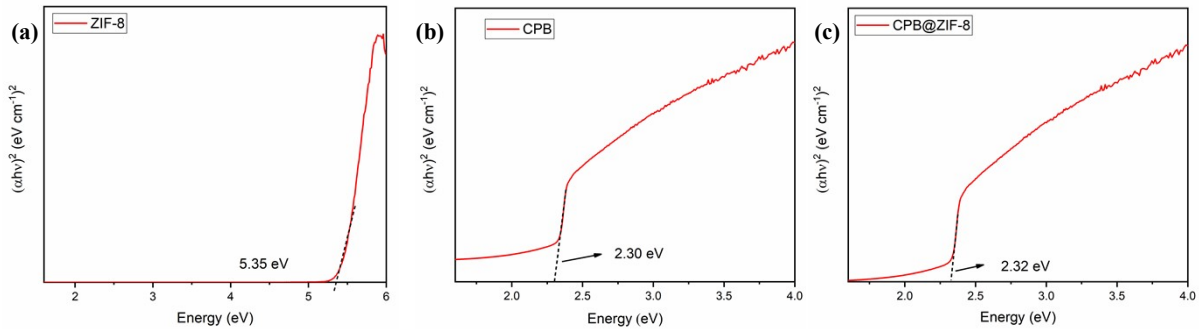

Figure S7: Optical band gap of (a) ZIF-8, (b) CPB, and (c)CPB/ZIF-8 calculated from Tauc plots.

Table S2: Calculated band gaps of ZIF-8, CPB, and CPB/ZIF-8

Material	**Absorption edge**	**Calculated Band Gap**
ZIF-8	210 nm	5.35 eV
CPB	512 nm	2.32 eV
CPB/ZIF-8	511 nm	2.32 eV

3) Electron paramagnetic resonance (EPR) Spectra of the ZIF-8 and CPB NCs

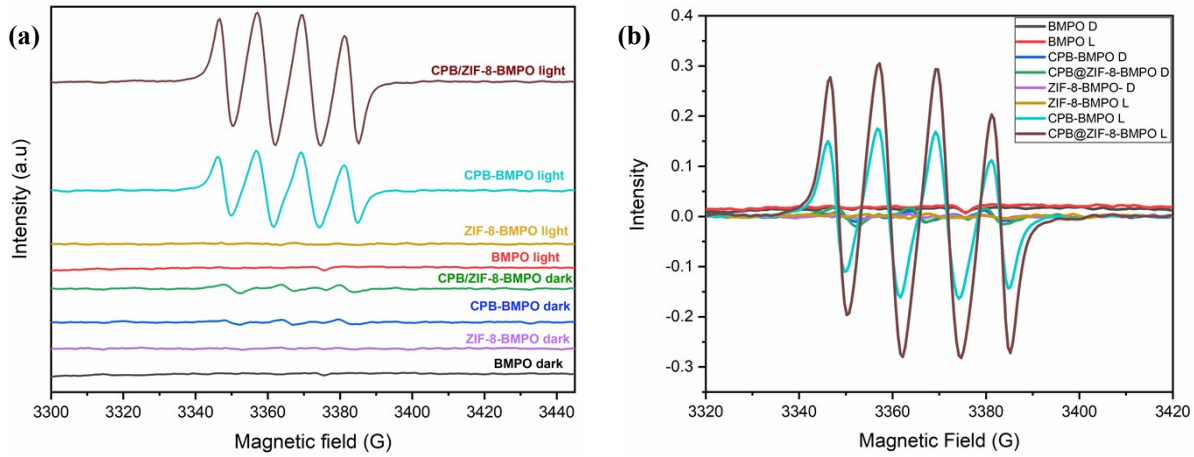

Figure S8: (a) The compiled EPR spectra of the materials under illumination and in the dark (b) compiled EPR spectra with values. (The graph in arbitrary units presents the EPR spectra under both dark and illuminated conditions, while the real intensity graph allows for a comparison of the spectral intensities of different samples under various experimental conditions)

$$ZIF\text{-}8 + h\nu \longrightarrow \text{No EPR signals}$$

$$CPB/ZIF\text{-}8 + h\nu \longrightarrow CPB/ZIF\text{-}8\ (e^- + h^+)\ \text{- Holes and electrons are generated in the presence of light}$$

$$O_2 + e^- \longrightarrow {}^{\bullet}O_2^-\ \text{- Electrons react with oxygen to form superoxide}$$

$$H_2O + h^+ \longrightarrow {}^{\bullet}OH + H^+\ \text{- Holes react with water molecules to form } {}^{\bullet}OH \text{ radicals causing strong EPR signals}$$

Addition of DMSO

$${}^{\bullet}OH + DMSO \longrightarrow {}^{\bullet}CH_3 + CH_3SOH\ (\text{Quenching of EPR signals due to the capture of } {}^{\bullet}OH \text{ radicals by DMSO})$$

Scheme S1. Schematic representation of the proposed mechanism of radical formation by ZIF-8 and the CPB/ZIF-8 composite, along with the scavenging of generated radicals using DMSO.

4) *Photocatalysis*

The analysis conditions are detailed in the Methods section of the main text. The kinetics of the degradation process were determined as follows:

A reaction kinetics study investigates how quickly the dye molecules break down under light exposure with a photocatalyst in a dye degradation reaction. To verify first-order degradation kinetics, we plotted the natural logarithm of the ratio of initial dye concentration to the concentration at a given time against time. The apparent rate constant (K_{aap}) was calculated using the following linear equation.[1]

$$ln(C_0/C_t) = K_{app}\, t \qquad (1)$$

Where C_0 *and* C_t represent the initial concentration and concentration at time t of dye, respectively, the apparent rate constant (K_{app}) is determined from the slope of the line when plotting $ln(C_0/C_t)$ against time.

a. Stability of Methyl Orange (MO) and Bromocresol Green (BCG) Dyes in the Dark and Under Illumination

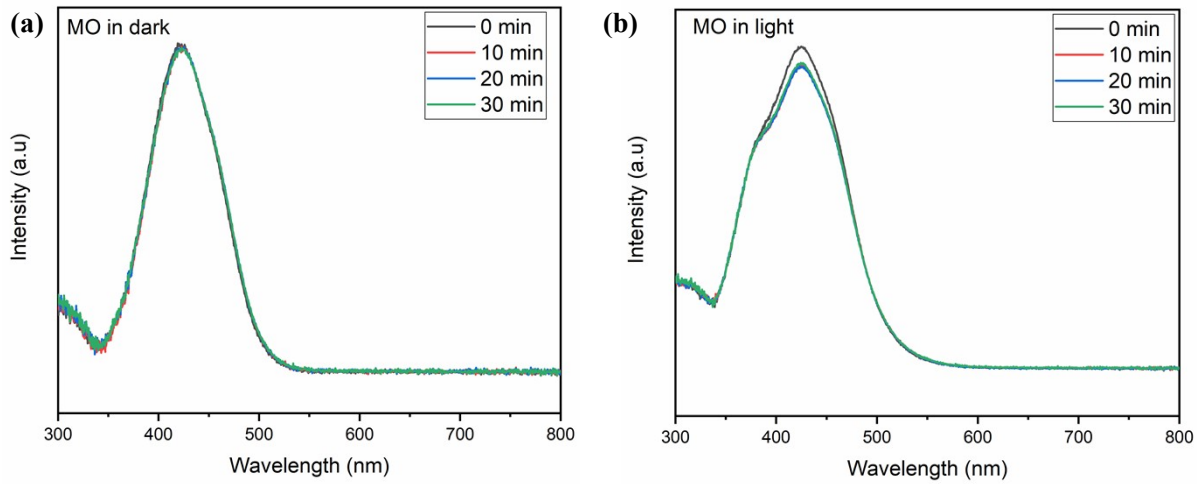

Figure S9: Time-dependent absorption spectra of MO dye under (a) dark and (b) under illumination. (This measurement was performed to confirm that the dyes remain stable in the solvent under both illuminated and dark conditions)

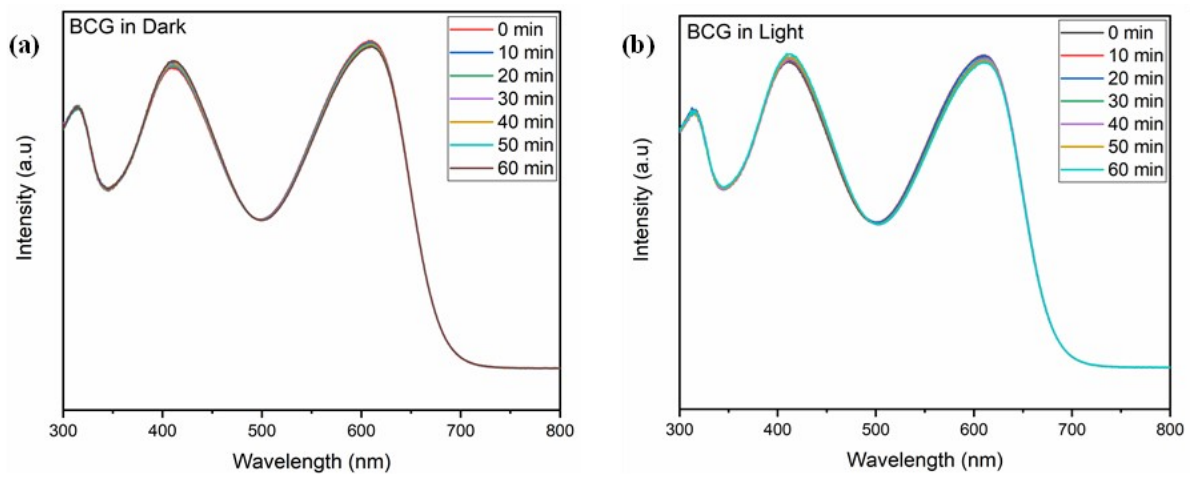

Figure S10: Time-dependent absorption spectra of BCG dye in (a) dark and (b) under illumination. (This measurement was performed to confirm that the dyes remain stable in the solvent under both illuminated and dark conditions)

b. Methyl orange (MO) degradation analysis

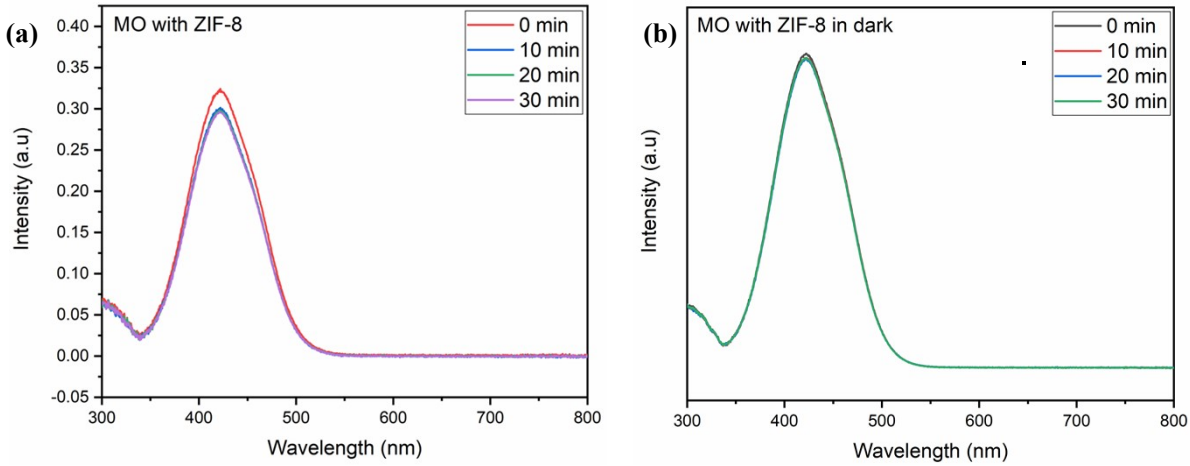

Figure S11: Time-dependent absorption spectra of MO dye with (a) ZIF-8 under illumination and (b) in dark. (This measurement was conducted to confirm the catalyst's activity by evaluating the degradation of the dye with the photocatalyst in the dark before illumination, enabling a comparison of the catalyst's performance under both dark and illuminated conditions)

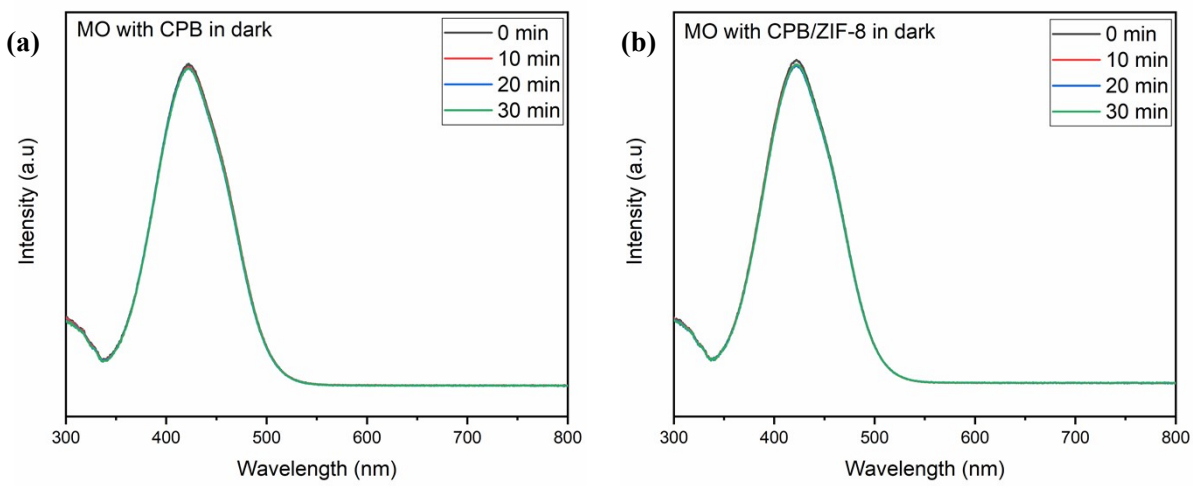

Figure S12: Time-dependent absorption spectra of MO dye with CPB/ZIF-8 in the dark. (This measurement was conducted to confirm the catalyst's activity by evaluating the degradation of the dye with the photocatalyst in the dark before illumination, enabling a comparison of the catalyst's performance under both dark and illuminated conditions)

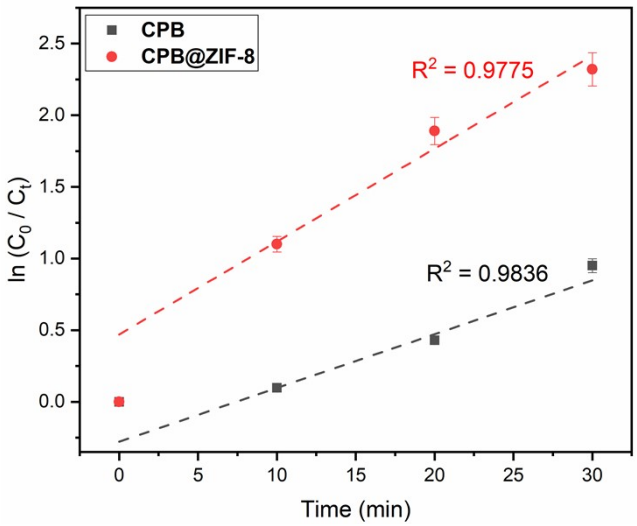

Figure S13: Kinetics plots of the CPB and CPB/ZIF-8

c. Bromocresol green (BCG) degradation

The photocatalytic activity of BCG was evaluated under both dark and illumination conditions. Due to the high pH dependency of BCG, the effect of the catalyst on the dye's pH was first assessed. The dye was mixed with the catalyst and stirred in the dark for 30 minutes, with measurements taken at 10-minute intervals. It was observed that the pH stabilized after 30 minutes. Therefore, during photocatalytic measurements under illumination, the dye was first stirred in the dark for 30 minutes to stabilize pH. The absorbance value of the dye after this 30-minute dark stirring period was considered the baseline (0 minutes) for dye degradation calculations.

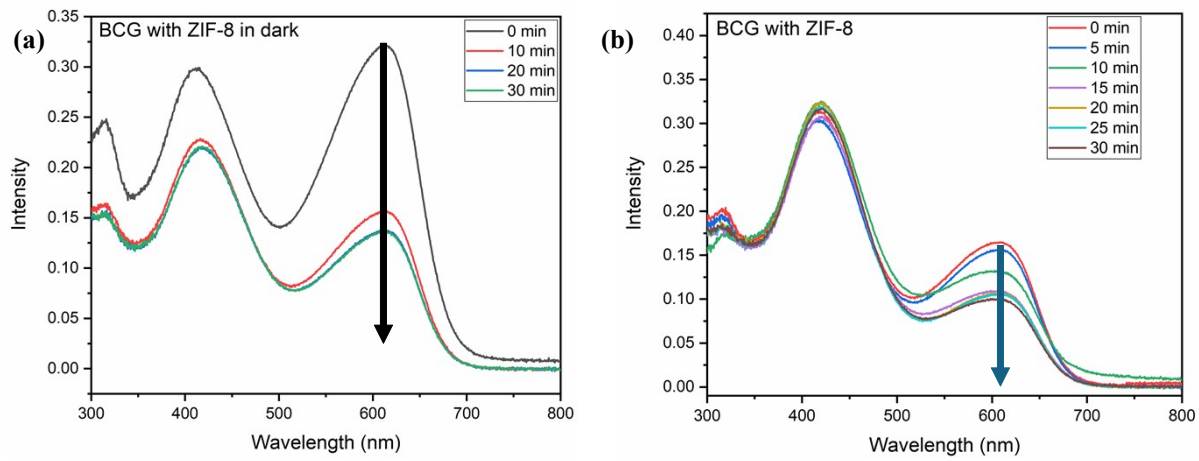

Figure S14: Time-dependent absorption spectra of BCG dye with ZIF-8 in (a) dark and (b) under illumination.

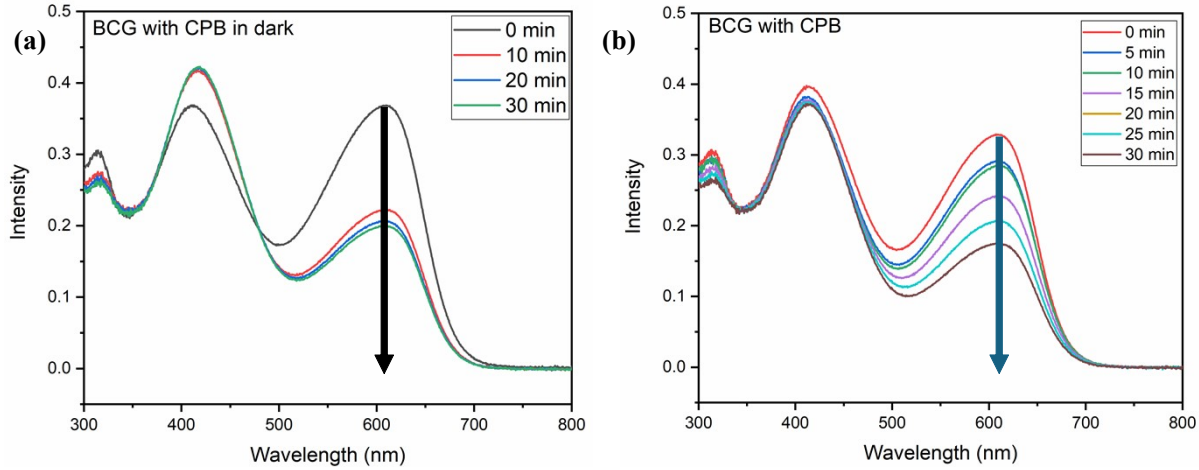

Figure S15: Time-dependent absorption spectra of BCG dye with CPB in (a) dark and (b) under illumination.

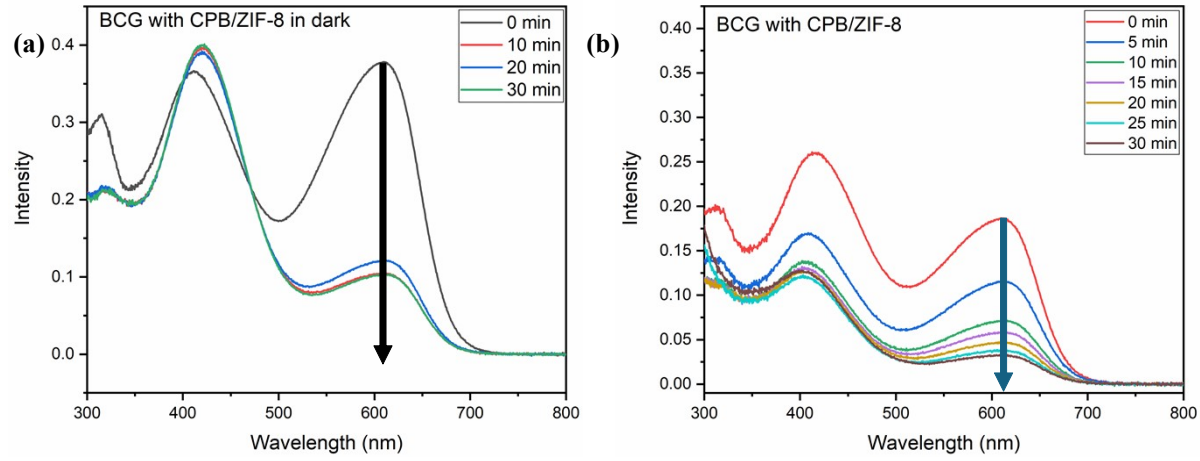

Figure S16: Time-dependent absorption spectra of BCG dye with CPB/ZIF-8 in (a) dark and (b) light conditions.

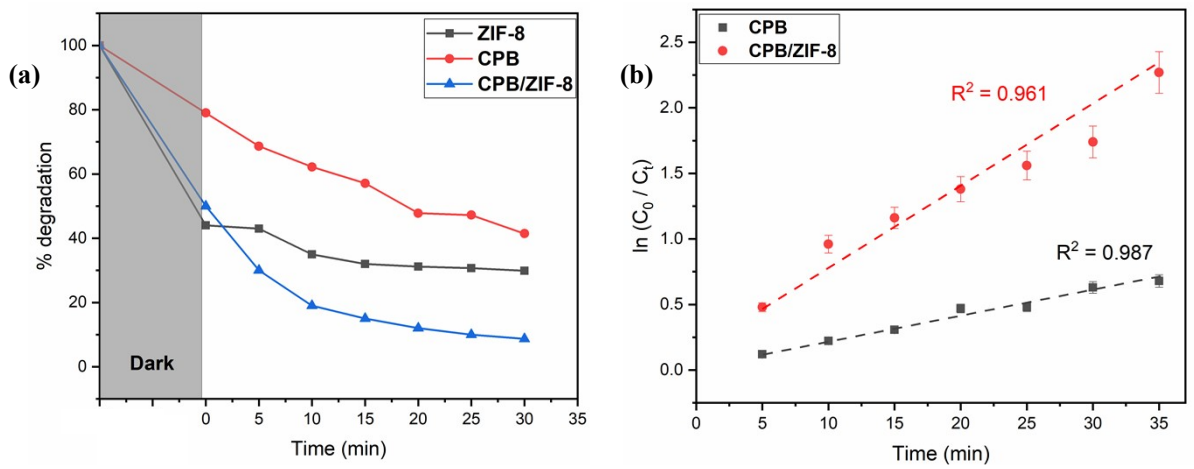

Figure S17: (a) Time-dependent degradation of BCG dye with different photocatalysts (b) kinetics plots of the CPB and CPB/ZIF-8

d. Possible degradation products for the dyes

The degradation pathways of MO under photocatalytic conditions begin with the cleavage of the azo bond (-N=N-), producing aromatic amines like sulfanilic acid and N, N-dimethyl-p-phenylenediamine.[2] This process can be monitored by analyzing the absorbance of MO, which shows a characteristic peak at 465 nm corresponding to the π-π* transition of the azo group. A decrease in this peak's intensity during degradation indicates cleavage of the azo bond.[2] Following this, hydroxyl radicals formed in the presence of a catalyst attack the benzene rings, leading to hydroxylated aromatic intermediates. These intermediates are oxidized, forming small aliphatic carboxylic acids, such as acetic, oxalic, and formic acids. The final step involves the complete mineralization of these acids into CO_2 and H_2O, effectively eliminating the dye pollutants.

A similar pathway is followed for bromocresol green (BCG), though with differences in intermediate formation. The process begins with the cleavage of the phenolic (-OH) and sulfonate ($-SO_3H$) groups by •OH radicals, which leads to ring opening and fragmentation. The oxidative degradation then forms aliphatic carboxylic acids, which are further oxidized into CO_2 and H_2O, completing the mineralization process.

In summary, both MO and BCG undergo oxidative degradation via •OH radicals, ultimately leading to the mineralization of the dyes into CO_2 and H_2O. This ensures the complete removal of dye pollutants from the system.

5) *Stability of the CPB and CPB/ZIF-8 under illumination and dark conditions*

A photostability test was conducted in a 10% ethanol-toluene (EtOH/toluene) solution to assess the stability of CPB NCs and CPB/ZIF-8 nanocomposites.[3] This experiment aimed to enhance the survivability of CPB NCs by leveraging the protective nature of the ZIF-8 framework. The samples were dispersed in the solvent mixture, and their photostability was evaluated under both dark and illumination conditions by monitoring the degradation of photoluminescence (PL) intensity over time.[4] PL spectra were recorded every 10 minutes for up to 30 minutes to track stability trends (**Figures S18 and S19**). The comparative analysis revealed that pristine CPB NCs exhibited 37% decomposition in the dark and 39% under illumination within 30 minutes. In contrast, CPB/ZIF-8 nanocomposites demonstrated significantly improved stability, with only 5% decomposition in the dark and 18% under illumination (**Figure S20**). These results confirm that CPB/ZIF-8 effectively enhances the stability of CPB NCs in the EtOH/toluene solution, significantly reducing the degradation rate compared to pristine CPB NCs.

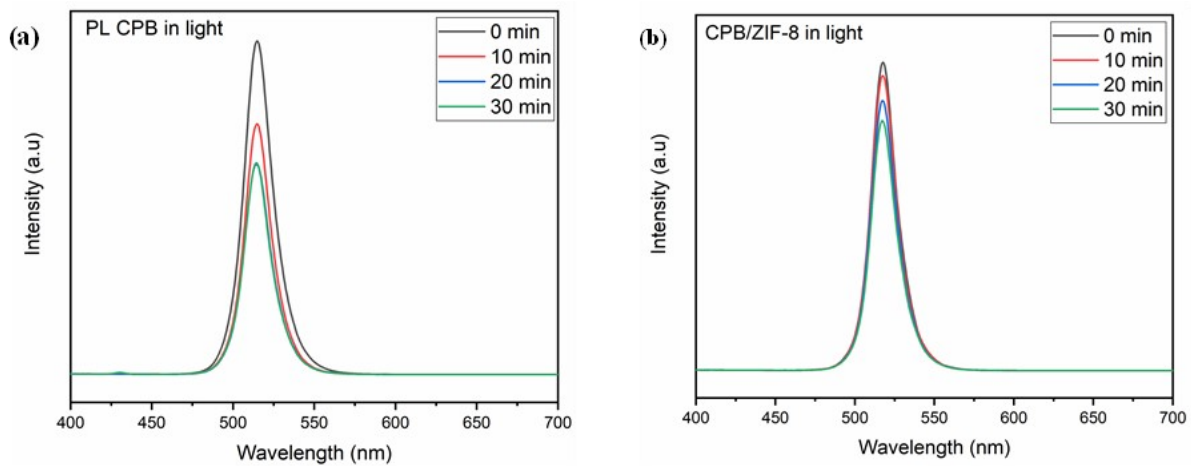

Figure S18: Time-dependent degradation of the PL intensity of the (a) CPB and (b) CPB/ZIF-8 in light conditions.

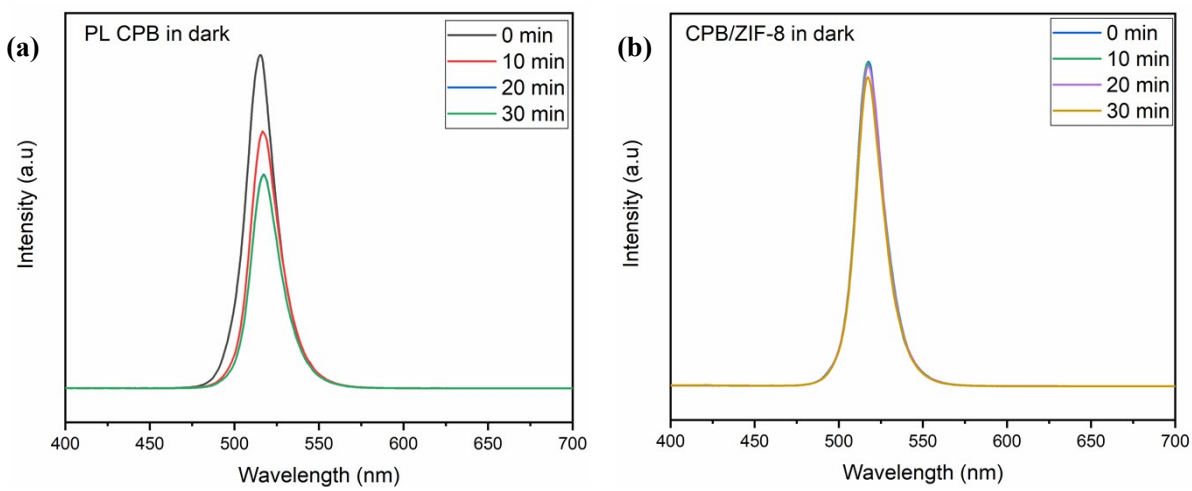

Figure S19: Time-dependent degradation of the PL intensity of the (a) CPB and (b) CPB/ZIF-8 in dark conditions.

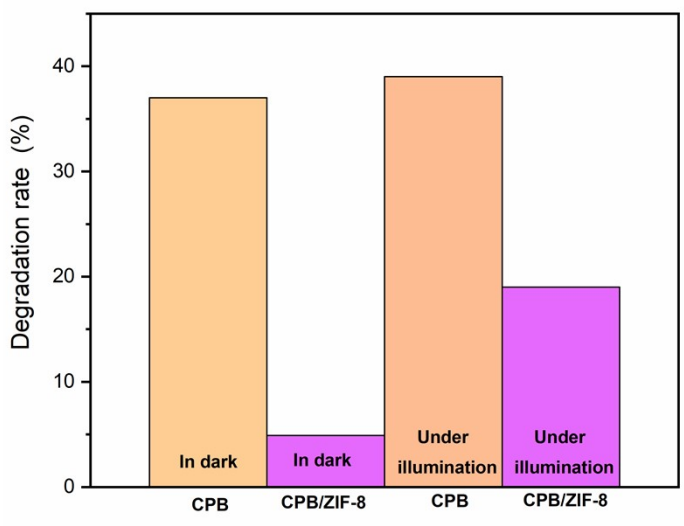

Figure S20: Degradation rate measured by evaluation of the decrease in the PL intensity of CPB and CPB/ZIF-8 under illumination and dark conditions after 30 minutes

6) *Structural and optical analysis of CPB/ZIF-8 composite synthesized via one-pot strategy (CPB/ZIF-8-OP).*

A one-pot synthesis strategy was employed to encapsulate the CPB within the ZIF-8 matrix by mixing all precursors in a single step. However, SEM analysis revealed the formation of aggregated structures rather than a well-defined ZIF-8 framework with uniformly dispersed CPB NCs. Moreover, the micrographs indicate that the CPB completely covers the ZIF-8, disrupting its structural integrity. This outcome contradicts the initial design, which intended for the CPB to be encapsulated within the ZIF-8. (Figure S21a). The FTIR spectrum of CPB/ZIF-8-OP exhibits a characteristic ZIF-8 peak at 420 cm^{-1}, corresponding to the Zn–N

bond (Figure S21b).[5] However, when examining the picks ascribed to the imidazole, distortions are observed in the peaks associated with C–H vibrations and C–N stretching. Notably, imidazole molecules ($(CH)_3(NH)N$) are the key components in the formation of the ZIF-8 structure. Therefore, any distortion or decrease in peak intensity clearly indicates structural disruption within its framework.[6] In comparison, the FTIR spectrum of the composite formed by ZIF-8 decorated with pre-prepared CPB NCs shows well-preserved characteristic imidazole peaks, indicating that the structural integrity of the framework is maintained. (Figure 3) To further understand and analyze the composites prepared by the two different methods (one-pot vs. post-decoration), we compared their optical responses. The CPB/ZIF-8-OP composite exhibited an absorption edge at 522 nm, whereas the CPB/ZIF-8-DNC, prepared by decorating ZIF-8 with pre-synthesized CPB NCs, showed a blue-shifted onset at 512 nm (Figure S22a). Notably, the latter aligns with the absorption edge of the pristine CPB NCs synthesized via the HI method.[7] The shift in the absorption in the CPB/ZIF-8-OP composite can be attributed to the formation of larger CPB particles compared to those obtained via the HI method. It may also result from the presence of additional phases, such as Cs_4PbBr_6.[8] Markedly, the composite displayed poor dispersion in a 10% (v/v) ethanol-toluene solvent mixture, restricting its suitability for photocatalytic degradation studies. The 'one-pot' synthesized composite exhibited inferior morphological, structural, and optical properties compared to the CPB-decorated ZIF-8. Consequently, we discontinued further photocatalytic experiments and characterization of this material.

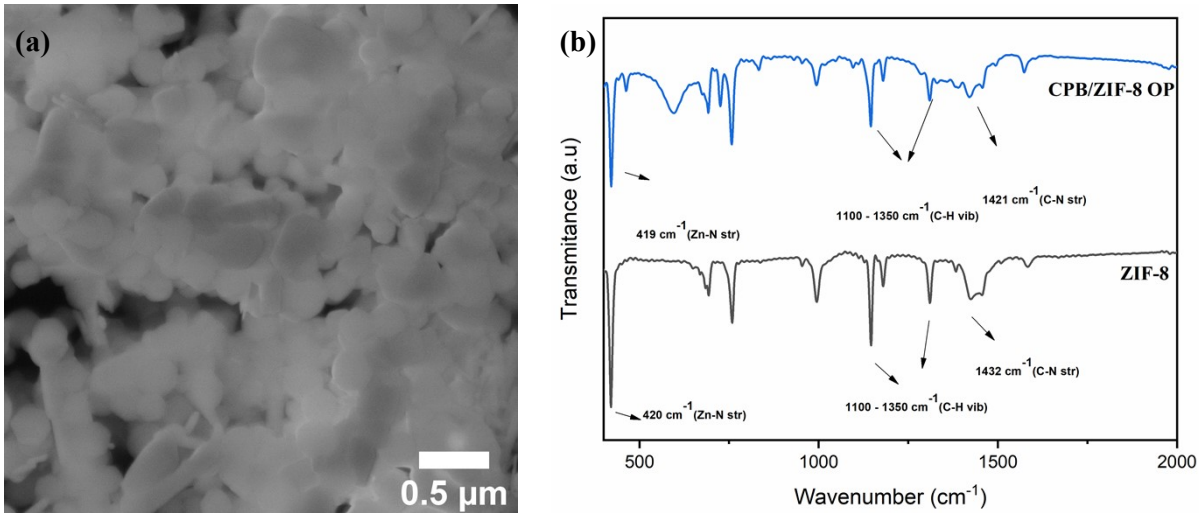

Figure S21: (a) The SEM micrograph of CPB/ZIF-8-OP composite (b) FTIR spectra of CPB/ZIF-8-OP compared to the pristine ZIF-8.

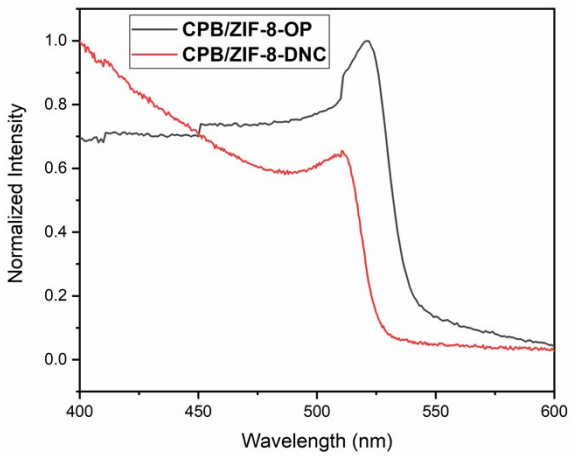

Figure S22: The UV spectra of the CPB/ZIF-8-OP and CPB/ZIF-8-DNC

7) Electrical energy consumption

The assessment of waste treatment as an effective method is significantly influenced by energy consumption. Notably, the degradation of organic contaminants through photocatalysis is closely linked to the primary operational expense: electrical energy. A critical metric in this context is the electrical energy per order (EE/O), which quantifies the amount of electrical energy (measured in kWh) needed to reduce the concentration of pollutants by 90% in one cubic meter of contaminated water. The EE/O value validates the required total power and facilitates a swift assessment of electrical energy expenditures. The EE/O of the CPB/ZIF-8 is calculated by equations 2 and 3.[9,]

$$UV\ Dose = \frac{Lamp\ power\ (kW) \times time\ (h) \times 1000}{Treated\ volum\ (L)} \quad (2)$$

$$EE/O = \frac{UV\ dose}{\log\ (Co/Ct)} \quad (3)$$

EE/O calculation for CPB/ZIF-8 for the degradation of MO

$$UV\ Dose = \frac{Lamp\ power\ (kW) \times time\ (h) \times 1000}{Treated\ volum\ (L)} = \frac{92.2 \times 10^{-6} \times 0.5 \times 1000}{0.025} =$$

1.844 kWh / L

$$EE/O = \frac{UV\ dose}{\log\ (Co/Ct)} = \frac{1.844}{\log\ (100/9.8)} = 1.83\ \text{kWh}/\text{m}^3$$

EE/O calculation for CPB for the degradation of MO

$$UV\ Dose = \frac{Lamp\ power\ (kW) \times time\ (h) \times 1000}{Treated\ volum\ (L)} = \frac{92.2\ \times 10^{-6} \times 0.5 \times 1000}{0.025} =$$

1.844 kWh / L

$$EE/O = \frac{UV\ dose}{\log\ (Co/Ct)} = \frac{1.844}{\log\ (100/39)} = 4.51\ \text{kWh /m}^3$$

EE/O calculation for CPB/ZIF-8 for the degradation of BCG

$$UV\ Dose = \frac{Lamp\ power\ (kW) \times time\ (h) \times 1000}{Treated\ volum\ (L)} = \frac{92.2\ \times 10^{-6} \times 0.5 \times 1000}{0.025} =$$

1.844 kWh / L

$$EE/O = \frac{UV\ dose}{\log\ (Co/Ct)} = \frac{1.844}{\log\ (100/16)} = 2.32\ \text{kWh /m}^3$$

EE/O calculation for CPB for the degradation of BCG

$$UV\ Dose = \frac{Lamp\ power\ (kW) \times time\ (h) \times 1000}{Treated\ volum\ (L)} = \frac{92.2\ \times 10^{-6} \times 0.5 \times 1000}{0.025} =$$

1.844 kWh / L

$$EE/O = \frac{UV\ dose}{\log\ (Co/Ct)} = \frac{1.844}{\log\ (100/64)} = 9.54\ \text{kWh /m}^3$$

8) Photocatalytic reaction efficiency or Quantum Efficiency (QE)

Quantum yield (QE), a measure of the product production or reactant disappearance rate relative to the number of absorbed photons per unit of time, is frequently used to assess the efficacy of the degradation process.[10,9] The QE of the dye degradation reactions was calculated by equation(4).

$$QE = \frac{(The\ number\ of\ pollutant\ molecules\ reduced\ (or\ degraded) in\ a\ given\ time\ )}{(total\ number\ of\ photons\ absorbed\ by\ the\ catalyst\ to\ be\ activated)}$$

(4)

a. Quantum Efficiency (QE) of CPB/ZIF-8

$$QE = \frac{(The\ number\ of\ pollutant\ molecules\ reduced\ (or\ degraded) in\ a\ given\ time\ )}{(total\ number\ of\ photons\ absorbed\ by\ the\ catalyst\ to\ be\ activated)}$$

Number of photons Np = Eλ/hc

Total number of photons = Np × irradiation time

QE= (6.51 X10^{17})/(4.61 X 10^{20}) = 1.41×10 $^{-3}$ molecules per photon

Table S3: Tabulated details regarding the calculation of the number of degraded pollutants (MO)

	Values
Number of pollutant moles in a solution	48 µM
The volume of the solution	25 mL
Number of pollutant molecules in a mole	6.02×10^{23} molecules/mole
Total number of pollutant molecules	$7.224 \text{ X } 10^{17}$ molecules
Percentage of degradation by CPB/ZIF-8	90.2%
Number of degraded pollutant molecules by CPB/ZIF-8	$6.51 \text{ X}10^{17}$ molecules

Table S4: Tabulated details regarding the calculation of the total number of photons and quantum efficiency.

	Values
λ = wavelength	550 nm
Photon energy	$3.6\text{X}10^{-19}$ J
Lamp power	0.0922 W
Irradiation time	1800 s
Total number of photons	$4.61 \text{ X } 10^{20}$ photons
Quantum efficiency of CPB/ZIF-8	1.41×10^{-3} molecules photon^{-1}

b. Quantum Efficiency (QE) of CPB

Table S5: Tabulated details regarding the calculation of the number Of degraded pollutants (MO)

	Values
Number of pollutant moles in a solution	48 µM
The volume of the solution	25 mL
Number of pollutant molecules in a mole	6.02×10^{23} molecules/mole
Total number of pollutant molecules	$7.224 \text{ X } 10^{17}$ molecules
Percentage of degradation by CPB	61%
Number of degraded Pollutant molecules by CPB	$4.40 \text{ X}10^{17}$ molecules

Table S6: Tabulated details regarding the calculation of the total number of photons and quantum efficiency.

	Values
λ = wavelength	550 nm
Photon energy	$3.6\text{X}10^{-19}$ J
Lamp power	0.0922 W
Irradiation time	1800 s
Total number of photons	$4.61 \text{ X } 10^{20}$ photons
Quantum efficiency of CPB	$0.98 \text{ X}10^{-3}$ molecules photon^{-1}

$$QE = \frac{(The\ number\ of\ pollutant\ molecules\ reduced\ (or\ degraded) in\ a\ given\ time\ )}{(total\ number\ of\ photons\ absorbed\ by\ the\ catalyst\ to\ be\ activated)}$$

Number of photons Np = Eλ/hc

Total number of photons = Np × irradiation time

*QE= (*4.40 X10^{17}*)/(* 4.61 X 10^{20} *) = 0.*98 X10^{-3} *molecules photon^{-1}*

c. Quantum Efficiency (QE) of CPB/ZIF-8 for BCG

Table S7: Tabulated details regarding the calculation of the number of degraded pollutants (BCG)

	Values
Number of pollutant moles in a solution	48 µM
The volume of the solution	25 mL
Number of pollutant molecules in a mole	6.02×10^{23} molecules/mole
Total number of pollutant molecules	7.224 X 10^{17} molecules
Percentage of degradation by CPB/ZIF-8	84%
Number of degraded Pollutant molecules by CPB/ZIF-8	6.08 X10^{17} molecules

Table S8: Tabulated details regarding the calculation of the total number of photons and quantum efficiency.

	Values
λ = wavelength	550 nm
Photon energy	3.6X10^{-19} J
Lamp power	0.0922 W
Irradiation time	1800 s
Total number of photons	4.61 X 10^{20} photons
Quantum efficiency of CPB	1.31 X10^{-3} molecules photon^{-1}

*QE= (*6.08 X10^{17}*)/(* 4.61 X 10^{20} *)* = 1.31 X10^{-3} *molecules photon^{-1}*

d. Quantum Efficiency (QE) of CPB for BCG

Table S9: Tabulated details regarding the calculation of the number of degraded pollutants (BCG)

	Values
Number of pollutant moles in a solution	48 µM
The volume of the solution	25 mL
Number of pollutant molecules in a mole	6.02×10^{23} molecules/mole
Total number of pollutant molecules	7.224 X 10^{17} molecules
Percentage of degradation by CPB	47%
Number of degraded Pollutant molecules by CPB	3.39 X10^{17}

Table S10: Tabulated details regarding calculating the total number of photons and quantum efficiency.

	Values

λ = wavelength	550 nm
Photon energy	$3.6X10^{-19}$ J
Lamp power	0.0922 W
Irradiation time	1800 s
Total number of photons	$4.61 X 10^{20}$ photons
Quantum efficiency of CPB	$0.73 X10^{-3}$ molecules $photon^{-1}$

QE= $(3.39 X10^{17})/(4.61 X 10^{20}) = 0.73 X10^{-3}$ *molecules* $photon^{-1}$

9) References

(1) Yusuff, A. S.; Taofeek Popoola, L.; Aderibigbe, E. I. Solar Photocatalytic Degradation of Organic Pollutants in Textile Industry Wastewater by ZnO/Pumice Composite Photocatalyst. *J. Environ. Chem. Eng.* **2020**, *8* (4). https://doi.org/10.1016/j.jece.2020.103907.

(2) Radini, I. A.; Hasan, N.; Malik, M. A.; Khan, Z. Biosynthesis of Iron Nanoparticles Using Trigonella Foenum-Graecum Seed Extract for Photocatalytic Methyl Orange Dye Degradation and Antibacterial Applications. *J. Photochem. Photobiol. B Biol.* **2018**, *183* (March), 154–163. https://doi.org/10.1016/j.jphotobiol.2018.04.014.

(3) Sedova, A.; Immanuel, P. N.; Carmieli, R.; Shalom, H.; Goldreich, A.; Thomas, A. S.; Prilusky, J.; Puravankara, A.; Bar-on, I.; Yadgarov, L. Exploring Halide Perovskite Nanocrystal Decomposition : Insight by in- Situ Electron Paramagnetic Resonance Spectroscopy. *Nano Res.* **2025**, *94907210*, 1–11. https://doi.org/https://doi.org/10.26599/NR.2025.94907210.

(4) Alam, A.; Li, Y.; Ning, F.; Li, T.; Wang, Y. Enhancing the Optical Properties and Stability of CsPbBr 3 Quantum Dots through Ligand Modification , Encapsulation, and Interaction with a Superhydrophobic Polymer. *ACS Appl. Mater. Interfaces* **2025**, 17026–17035. https://doi.org/10.1021/acsami.4c21351.

(5) Lee, Y. R.; Jang, M. S.; Cho, H. Y.; Kwon, H. J.; Kim, S.; Ahn, W. S. ZIF-8: A Comparison of Synthesis Methods. *Chem. Eng. J.* **2015**, *271*, 276–280. https://doi.org/10.1016/j.cej.2015.02.094.

(6) Talukder, N.; Wang, Y.; Nunna, B. B.; Tong, X.; Lee, E. S. An Investigation on the Structural Stability of ZIF-8 in Water versus Water-Derived Oxidative Species in Aqueous Environment. *Microporous Mesoporous Mater.* **2024**, *366* (November 2023), 112934. https://doi.org/10.1016/j.micromeso.2023.112934.

(7) Brennan, M. C.; Herr, J. E.; Nguyen-Beck, T. S.; Zinna, J.; Draguta, S.; Rouvimov, S.; Parkhill, J.; Kuno, M. Origin of the Size-Dependent Stokes Shift in CsPbBr3 Perovskite Nanocrystals. *J. Am. Chem. Soc.* **2017**, *139* (35), 12201–12208. https://doi.org/10.1021/jacs.7b05683.

(8) Sun, W.; Hung, Y. T.; Huang, W. T.; Liu, R. S.; Zhou, W. Photoluminescent Nano-CsPbBr3 Embedded in Cs4PbBr6 Crystals: Formation Mechanism and Properties. *Cryst. Growth Des.* **2024**, *24* (1), 545–553. https://doi.org/10.1021/acs.cgd.3c01226.

(9) Elbadawy, H. A.; Elhusseiny, A. F.; Hussein, S. M.; Sadik, W. A. Sustainable and Energy-Efficient Photocatalytic Degradation of Textile Dye Assisted by Ecofriendly Synthesized Silver Nanoparticles. *Sci. Rep.* **2023**, *13* (1), 1–13. https://doi.org/10.1038/s41598-023-29507-x.

(10) Sundar, K. P.; Kanmani, S. Progression of Photocatalytic Reactors and Its Comparison : A Review. *Chem. Eng. Res. Des.* **2019**, *154*, 135–150. https://doi.org/10.1016/j.cherd.2019.11.035.